Rationalized Computer-Aided design of Matrix Metalloprotease-Selective Prodrugs

Mohit Jain[1], J. Jonathan Harburn[1], Jason H. Gill[1], Paul M. Loadman[2], Robert A. Falconer[2], Caitlin A. Mooney[3], Steven L. Cobb[3], David J. Berry[1]*

[1]School of Medicine, Pharmacy and Health, Durham University, Queen's Campus, Stockton on Tees, TS17 6BH, UK.

[2]Institute of Cancer Therapeutics, ICT building, University of Bradford, Bradford, BD7 1DP, UK.

[3]Department of Chemistry, Durham University, Lower Mountjoy, South road, Durham, DH1 3LE, UK.

Protease, *in silico* modelling, Matrix Metalloproteinase

ABSTRACT: Matrix metalloproteinases (MMPs) are central to cancer development and metastasis. They are highly active in the tumour environment and absent or inactive in normal tissues; therefore they represent viable targets for cancer drug discovery. In this study we evaluated *in silico* docking to develop MMP-subtype-selective tumour-activated prodrugs. Proof of principle for this therapeutic approach was demonstrated *in vitro* against an aggressive human glioma model, with involvement of MMPs confirmed using pharmacological inhibition.

INTRODUCTION

Matrix Metalloproteinases (MMPs) are zinc-dependent endoproteases central to digestion of extracellular matrix (ECM) and pericellular proteins involved in regulation of many normal physiological processes including tissue growth and embryogenesis.[1-5] Their activity is regulated by both post-secretion zymogenic activation and inhibition by endogenous inhibitors termed TIMPs (tissue inhibitor of metalloproteinase).[6] However, dysregulation of MMP expression and unbalanced endoproteolytic activity of specific MMPs are a major contributor to many degradative diseases including arthritis, cancer, cardiovascular disease, inflammatory disorders, and neurodegeneration,[5,7-9] thus making them attractive drug targets.[2, 10, 11]

In the last two decades significant drug discovery effort was focused on inhibition of MMPs as a strategy to prevent tumour invasion and subsequent tumour metastases.[12] As a result the pharmaceutical industry produced a number of well tolerated orally active MMP inhibitors (MMPi).[13] These agents were largely peptidomimetic zinc-binding hydroxamates, based upon an MMP peptide substrate.[2,14,15] Although many of these inhibitors progressed to late stage clinical trials against metastatic cancer, limited clinical success was seen due to a lack of inhibitor MMP-subtype specificity and insufficient knowledge about the complexity of the disease biology.[2,16,17] Several additional strategies have been evaluated over recent years, including development of inhibitors exploiting the enzymatic transition state,[2,18] inhibitors binding enzyme cavity subsites,[19] or

alternative zinc chelation groups.[2] Generation of MMP sub-family-selective inhibitors still proves mostly elusive however, because of the broad structural similarity of their active site, substrate complexity, and identification of specific MMPs as anti-targets.[2,17]

In contrast to inhibition of MMP function, exploitation of the MMP-mediated proteolysis within diseased tissues has also been investigated as a diagnostic and prognostic approach. These studies used activity-based probes comprising a 'broad-spectrum' or selective MMP-cleavable peptide labelled with a quenched fluorophore or imaging moiety.[20,21] In this approach, elevated MMP activity in the diseased tissue results in activation of the probe via selective cleavage of the peptide and release of the contrast agent, facilitating imaging and quantification of MMP activity.[20,21]

In line with the MMP-activated probe-based approaches, elevated activity of MMPs within diseased tissue has also been explored as a strategy for conversion of a non-toxic peptide-conjugated prodrug into a potent therapeutic entity within the disease site. The advantage of this approach is dose intensification and reduced systemic drug exposure.[1,22-26] A requirement for success in activity-probes, prodrugs, or theranostic approaches is MMP-selectivity through incorporation of MMP-subtype unique (e.g. MMP-2, MMP-9 or MMP-14) peptide sequences and subsequent disease-selective activation.

The rationale for this study is to exploit the MMP binding subsites and modify the substrate residues to produce a pro-

1

drug selective for MMP-2 over MMP-9 and MMP-14, and create a robust approach which could be exploited for development of endoprotease-activated diagnostic probes and therapeutics. Visualizing and quantifying binding preferences and motifs can provide valuable insight into the structural determinants of substrate selectivity and enable MMP-targeted drug development.[27] In order to achieve this the following steps were undertaken; definition of the catalytic domains within the relevant MMPs through *in silico* study, docking of known MMP-selective sequences to highlight key catalytic binding determinants, subsequent rational design of novel MMP-selective prodrugs, and *in vitro* confirmation of MMP-selectivity and therapeutic proof-of-concept. In this work a reiterative approach using *in silico* proteolytic docking coupled to *in vitro* biochemical assessment has been applied to enable the development of prodrugs that are selectively activated by MMP-2 over MMP-9, the closely related gelatinase family members; and over MMP-14 – the endogenous activator of MMP-2. The availability of three-dimensional crystal structures of MMPs allowed us to critically examine the differences existing between the catalytic domains of the MMP-2 (PDB ID: 1QIB), MMP-9 (PDB ID ID: 1GKC) and MMP-14 (PDB ID: 1BQQ).[28,29,30] This allowed for successful development of *in silico* models of MMPs. The *in silico* model was able to accurately predict known cleavage sites on substrates and prodrugs by MMPs, thus enabling rationalized design of an MMP-2 selective peptide.

RESULTS AND DISCUSSION

The catalytic domain of MMPs consists of five β-sheet strands and three α-helices. The catalytic centre comprises of a catalytic zinc ion coordinated by three histidine residues and a glutamic acid.[28] The specificity loop within the catalytic site of MMPs shows the largest structural differences, as visualized for MMP-2 and MMP-9 in Figure S1. The overall folding of MMP-2 and MMP-9 resembles those of other MMPs, which is expected based on their structural similarity (Figure S1).[31] The cavity of S1' pockets in MMPs is well-suited to accommodate a wide-range of hydrophobic residues, with the main functional difference between MMP subtypes lying in this region. In MMP-9, residues 421–423 form the wall of the binding pocket and the specificity loop is formed by the residues 424 – 430. Arg424 is present at the bottom of S1' pocket and closes off the end. Arg424 is therefore responsible for making the pocket cavity smaller in MMP-9 than in MMP2 (Figure S1). Whereas in MMP-2, the external wall of the S1' pocket is largely formed by Thr227–Phe232 specificity residues, creating a deeper pocket. These differences can potentially be exploited for rational design of MMP-selective substrates/conjugates.

To probe the selective binding of potential substrates the peptide sequence of the non-specific gelatinase substrate **1** Dnp-Pro-β-cyclohexyl-Ala-Gly-Cys(Me)-His-Ala-Lys(N-Me-Abz)-NH$_2$ (M-2055)[32] was input into BIOVIA Discovery Studio 4.0, minimized with respect to its geometry, and then docked into the MMPs. In order to validate modelling work, attempts at crystallization of this and other substrates were undertaken in order to determine the X-ray crystal structure. Crystallization experiments failed to yield suitable crystals for structure determination, therefore only force field (CHARMM) minimized geometries of the substrates were employed throughout this study.

Figure 1 shows the interaction of **1** peptide sequence with human MMP-2 and MMP-9. In both MMPs the zinc ion interacts with the Gly and Cys(Me) bond, the known cleavage site

according to Bickett et al.[32] MMP-9 is able to bind tightly with the substrate residues compared to MMP-2, as determined by differences in their predicted inter-atomic zinc distances and overall binding energies. The substrate bound MMP-complexes provided crucial insight into the differences in their subsite interactions, as S1 and S3 subsites in MMP-2 demonstrated affinity to accommodate longer side-chains than MMP-9. The charged nature of the S2 subsite (presence of His205) in MMP-2 lends affinity for acidic residues, whereas this feature is not observed in MMP-9. In the MMP-9 structure, the carboxylic acid between Gly and Cys(Me) chelates the zinc ion (2.1 Å) and is involved in a strong H-bond to the carboxylate O of Glu402. The zinc ion is further coordinated by three Histidine residues namely His401, His405 and His411 present in Helix αβ segment of the protein. Only the P1' amino acid is involved in strong H-bonds with Arg424 (2.2 Å), which creates the wall-forming segment. The strong binding of Arg424 with the P1' residue is an important determinant of the specificity pocket. Remaining substrate residues are involved in strong interactions with the bulge-edge segment molecules (Gly186 to His190) with interatomic distances ranging from 2.5 to 3.1 Å. The docked complex of **1** and MMP-9 has an overall binding energy of 706 kcal/mol (Figures 1,S2, S3 and S4).

Consideration of the interaction of **1** with the active site of MMP-2 shows a marked reduction in affinity in energetic terms, the predicted interaction is seven times weaker than that of **1** and MMP-9 (binding energy of 101 kcal/mol). Gly forms the P1 subsite and Cys(Me) forms the P1' subsite and the presence of a zinc ion, chelated by the carboxylic acid between P1-P1' residues (3.8 Å), further confirms this. The P1' residue, although favourable for the MMP-2 specificity
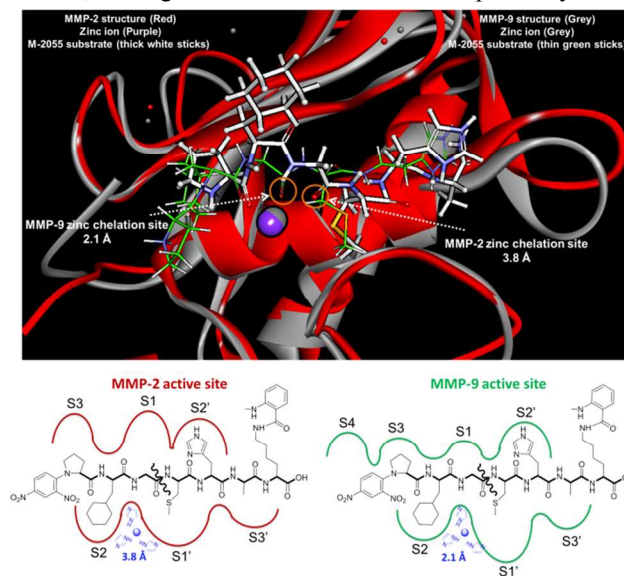

Figure 1. (Top) Stereo view of the docked complexes of **1** substrate and the catalytic domain of human MMP-2 (PDB ID: 1QIB) and MMP-9 (PDB ID: 1GKC). The MMP-substrate docked complexes are merged with zinc as the same point of view. MMP-2 structure is shown in red, zinc as purple and **1** substrate (white sticks) docked within MMP-2 active site. MMP-9 is shown in grey, zinc as green and **1** substrate (thin green sticks) docked within its active site. (Bottom) Schematic representation of **1**: active site binding interaction in human MMP-2 and MMP-9. MMP-2 and MMP-9 enzyme binding pockets are shown in red and green respectively. Substrate chemical structure and its scissile bond is shown in black. The zinc ion is indicated in blue.

pocket, is not involved in any significant interaction with MMP-2 residues. The remaining substrate residues have weak H-bond interactions with wall-forming and bulge-edge segments of MMP-2 with interatomic distances ranging from 3.1 to 5.1 Å. This is expected as **1** residues are oriented away from further MMP-2 binding pockets (Figure 1, S2, S3 and S4). Key observed differences between the binding affinity of MMP-2 and MMP-9 with **1** are: S1 and S3 subsites in MMP-2 can accommodate longer side-chains than MMP-9. Charged nature of S2 subsite in MMP-2 has affinity for acidic residues, whereas this feature is not observed in MMP-9. Refer to figure S5 for *in silico* binding of **1** with the active site of MMP-14, also demonstrating zinc interaction between Gly-Cys(Me) bond.

To experimentally validate the predictability of this model, and confirm the *in vitro* cleavage position of **1**, hydrolysis of the substrate by recombinant MMP-2 and MMP-9 was assessed over a 12 hour period. The resultant products were analysed by LCMS using a reverse phase gradient system to separate the substrate **1** and proteolytic products. The identification of these species was confirmed by retention time and mass spectrometry (MS) data. **1** demonstrated a retention time (tR) of 2.8 minutes (Figure S6) and rapid cleavage by MMP-9 at Gly-Cys(Me) bond was confirmed by LCMS, two peaks corresponding to Dnp-Pro-β-Cyclohexyl-Ala-Gly at tR of 2.3 minutes (m/z 491.5Da, [M+H]+) and Cys(Me)-His-Ala-Lys(N-Me-Abz)-NH2 at tR of 2.47 minutes (m/z 604.7Da, [M+H]+) (Figures 2 and S7). Slow hydrolysis of **1** by MMP-2 (compared to MMP 9) at Gly-Cys(Me) bond was confirmed by two peaks at tR of 2.3 minutes and tR of 2.47 minutes. MMP-2 cleavage experiments displayed a parent peak of **1**, detected at tR of 2.8 minutes (m/z 1077.5Da, [M+H]+), suggesting that MMP-2 metabolised **1** at a slower rate than MMP-9 (Figures 2 and S8). Recombinant MMP-14 also cleaved **1** at the Gly-Cys(Me), confirming the *in silico* prediction (Figure S9). This *in vitro* assessment supports the validity of the predicted *in silico* model of substrate and MMP interactions and was subsequently used for further design of MMP-targeted therapeutics.
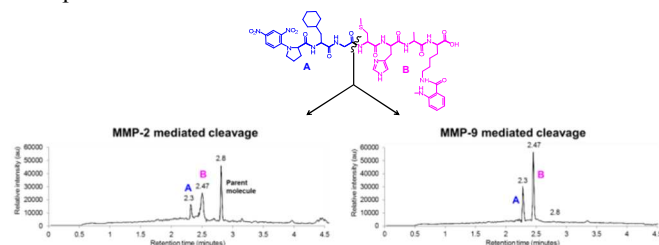

Figure 2. Schematic representation of the cleavage of **1** substrate by recombinant MMP-2 and MMP-9 enzymes at Gly-Cys(Me).

The next phase of the study was to design a prodrug (substrate and warhead) which would be selectively activated by a specific MMP over a close family homologue i.e. cleaved by MMP-2 and not by MMP-9 or MMP-14. A known MMP-targeted peptide-conjugated doxorubicin prodrug[33,34] was evaluated as it is cleaved by MMP-2, MMP-9 and MMP-14, presenting an excellent model for further modification. MMP-targeted peptide-conjugates were synthesized via solid phase chemistry and purified by reverse phase HPLC, the chemotherapeutic drug doxorubicin conjugated to the C-terminus (Scheme S10). *In silico* interaction of the **2** (reference compound) with MMP-2 and MMP-9 shows the zinc ions are che-

lated by the carboxylate between Gly-Ser(O-Benzyl) bond (2.6 Å and 2.8 Å respectively), the known cleavage site.[31,32] Figure S11 shows the binding pockets of MMP-2 are larger and deeper than MMP-9, S1 subsite allowing for larger aromatic residues. The compound **2** aligns tightly into the active site of both MMPs as shown by their predicted interatomic zinc distances and binding energies (555 kcal/mol and 492 kcal/mol) in MMP-2 and MMP-9 docked complexes respectively. Active site residues interact with the compound in a similar way to that previously explained. His205 in MMP-2 αβ-Helix loop makes the S2 pocket charged in nature and could potentially accommodate acidic residues (Figures S11 and S12). Similar to MMP-2 and MMP-9, MMP-14 also demonstrated selective interaction with **2** (Figure S13) To experimentally validate the *in silico* docking of **2**[33,34] and confirm the *in vitro* cleavage site, the lysis of this prodrug by recombinant MMP-2 and MMP-9 was assessed over a 12 hour period; with the resultant products being assessed by LCMS. HPLC (reverse phase gradient) was used to separate **2** (Cbz-Glu-Pro-Leu-Gly-Ser(O-Benzyl)-Tyr-Leu-Doxorubicin),[33,34] identification confirmed by mass spectrometry (MS) with a retention time (tR) of 3.63 minutes (Figure S14). Cleavage of **2** by both MMP-2 and MMP-9 at Gly-Ser(O-Benzyl) bond was confirmed by LCMS, two peaks corresponding to Cbz-Glu-Pro-Leu-Gly at tR of 2.87 minutes (m/z 547.2Da, [M+H]+) and Ser(O-Benzyl)-Tyr-Leu-Doxorubicin at tR of 3.23 minutes (m/z 997.4, [M+H]+). (Figures 3, S15 and S16). A parent peak was also detected at tR of 3.63 minutes (m/z 1525.8Da, [M+H]+). Similarly, MMP-14 also displayed hydrolysis of **2** at the Gly-Ser(O-Benzyl) bond (Figure S17). This *in vitro* assessment supports the predictability of *in silico* model of anticancer therapeutics with MMPs, for further design of MMP-2 selective prodrugs.
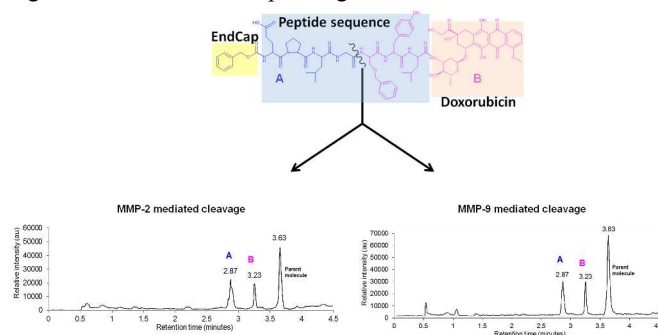

Figure 3. Schematic representation of the cleavage of **2** by recombinant MMP-2 and MMP-9 enzymes at the Gly-Ser(O-Bn) bond.

Rational design of a peptide conjugate selective for MMP-2 over MMP-9 was achieved by incorporating residues into the peptide chain to fit S1, S2, S3 and S1' pockets of MMP-2 which differ in size and polar affinity compared to MMP-9. The following modifications were incorporated: Aromatic residues in S1 subsite; acidic side-chain in S2 subsite and a polar side-chain at the S3 subsite. Small non-polar residues were included at the S1' subsite despite S1's potential to accommodate longer hydrophobic residues. This was due to longer residues leading to a negative effect on the predicted binding affinity, due to conformational alteration.
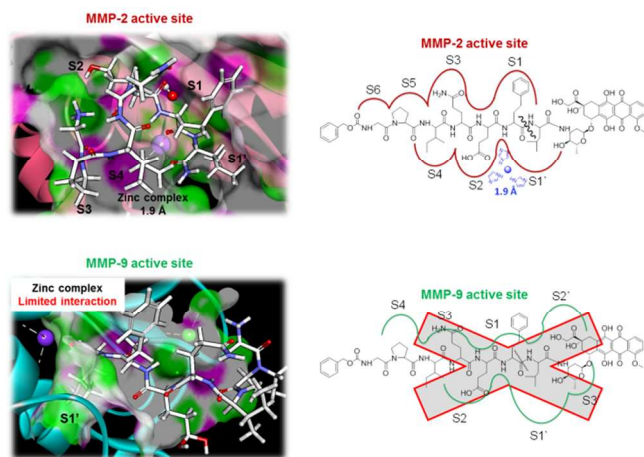
Figure 4. (Left) Stereo view of docked complexes of **3** (white sticks), catalytic domain of human MMP-2 (PDB ID: 1QIB) (Red) and MMP-9 (PDB ID: 1GKC) (Green). Catalytic and structural zinc ions are shown as purple spheres and active-site cleft residues (αβ-helix loop and the specificity loop) are shown as green. (Right) Schematic representation of **3** substrate: active site binding interaction in MMP-2 and MMP-9, are shown in red and green respectively. Substrate chemical structure and its scissile bond is shown in black and zinc ion coordinated by histidine is indicated in blue.

The zinc ion in MMP-2 demonstrated interaction with **3** at carboxylate between Homophenylalanine (Hof)-Leu bond (1.9 Å), indicating the predicted cleavage site. Residues of MMP-2 tightly bind with **3** as demonstrated by strong interactions with the bulge-edge segment molecules (Gly162 to His166) and the wall-forming segment molecules (Tyr223 to Thr229) with interatomic distances ranging from 1.8 to 2.8 Å. The docked complex of **3** and MMP-2 has an overall binding energy of 805 kcal/mol. In MMP-9 the zinc interaction is not detectable and the predicted binding energy is negative (-107 kcal/mol) suggesting the modified peptide residues should give selectivity of MMP-2 over MMP-9 (Figures 4, S18 and S19). Similarly, based on the peptide modifications for MMP-14 selectivity suggested in the literature,[35,36] the zinc interaction between **3** and MMP-14 was non-detectable and the binding energy was negative (Figure S20). The hydrolysis of **3** by recombinant MMP-2, MMP-9 and MMP-14 was assessed over a 12 hour period and analyzed by LCMS. Reverse phase HPLC identified **3** at tR of 3.58 minutes (Figure S21). **3** was preferentially cleaved by MMP-2 at Hof-Leu and two peaks were identified; corresponding to Leu-Doxorubicin at tR of 2.078 minutes (m/z 657.2Da, [M+H]+) and Cbz-Gly-Pro-Ile-Gln-Glu-Hof at tR of 2.826 minutes (m/z 821.4Da, [M+H]$^+$) (Figures S22 and S23). Conversely MMP-9 and MMP-14 did not cleave **3** in the same timeframe, indicating that **3** is MMP-2 selective supporting the *in silico* prediction (Figure S22 and S24).

In order to assess activity and demonstrate proof-of-concept for the developing approach, the effects of **3** were assessed against the U87-MG malignant human glioma cell line. This cell line is derived from a highly aggressive glioma tumour and expresses both MMP-2 and MMP-9 (Figure 5). Cytotoxicity was observed in this cell line with doxorubicin, Leucine-doxorubicin (Leu-Dox) and **3**, with IC50 values of 0.3±0.2 μM, 0.6±0.2 μM and 5.0±1.2 μM, respectively. The differential cytotoxicity between doxorubicin and **3** supports the requirement for **3** to be activated prior to inducing its effects. Furthermore, **3** remained inactive in the presence of a pan-

MMP inhibitor, (2R)-N'-hydroxy-N-[(2S)-3-(1H-indol-3-yl)-1-(methylamino)-1-oxopropan-2-yl]-2-(2-methylpropyl)butanediamide (GM6001; Ilomastat/Galardin),[37] demonstrating MMP-selective chemotherapeutic action of this prodrug.

In order to further determine the tumour-selective activation of **3**, its metabolism was studied *ex vivo* using MMP-expressing HT1080 human tumour xenograft[33], mouse plasma and homogenized murine liver and kidney tissues (Figure S25). Rapid metabolism of **3** was observed in the HT1080 xenograft homogenate ($t_{1/2}$ = > 8.8 minutes). In comparison, **3** was relatively stable in plasma ($t_{1/2}$ = significantly > 90 minutes), murine liver ($t_{1/2}$ = > 17.0 minutes) and murine kidney ($t_{1/2}$ = > 38.1 minutes). The liver homogenate is a 'worse case scenario' for **3**'s stability due to a high proportion of both extracelluar and intracellular proteases. **3** displayed relative stability in mouse plasma and liver and kidney homogenates, and associated rapid metabolism in tumour homogenates.
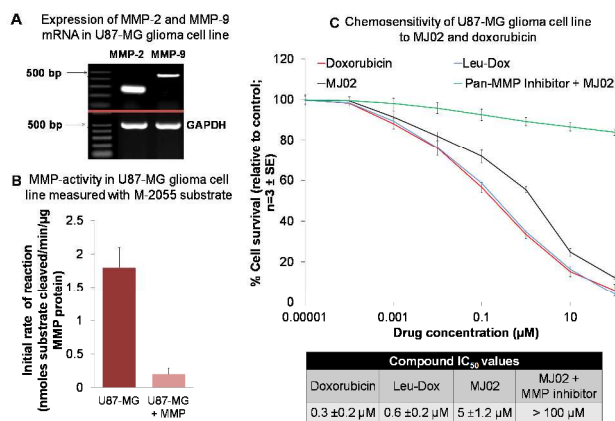

Figure 5. Therapeutic activity of **3** against human cancer. A) Expression of MMP-2 and MMP-9 mRNA in the U87-MG glioma cell line; B) MMP-activity in the U87-MG cell line, as demonstrated by activation of **1** substrate Dnp-Pro-β-cyclohexyl-Ala-Gly-Cys(Me)-His-Ala-Lys(N-Me-Abz)-NH₂; C) Cytotoxicity of doxorubicin, Leu-Dox and **3** against U87-MG cell line. MMP-selective activation of **3** in the presence of a pan-MMP inhibitor (Ilomastat).

CONCLUSIONS

Targeted cancer therapies offer the potential of reduced side effects along with benefits of prolonging drug exposure to cancerous tissues, enabling improved tumour response and survival rates.[38,39] Harnessing the elevated enzymatic activity of MMPs within the tumour microenvironment to selectively convert a non-toxic prodrug into a potent chemotherapeutic agent is one such approach with significant potential therapeutic scope.[40,41] In this study a reiterative approach using *in silico* docking coupled to *in vitro* biochemical proteolytic assessment have been applied to enable the development of anti-cancer prodrugs selectively activated by MMP-2, but not by close family homologue-MMP-9 or the MMP-2 activator MMP-14. Proof-of-concept for this therapeutic approach was demonstrated against a glioma cell line *in vitro*, with the involvement of MMPs confirmed using pharmacological inhibition and by tumour-selective activation with *ex vivo* tumour xenografts. This study has shown that it is feasible to utilise *in silico* predictive approaches to rationally design MMP-

selective prodrugs with possible utility in the treatment of cancer.

EXPERIMENTAL

3D-Molecular Modelling

Refer to Method S30

Synthesis of MMP-targeted peptide conjugates

Custom designed peptide sequences with Cbz (Benzyloxycarbonyl) as the chemical endcap were supplied (Bachem, Switzerland)/ synthesised using solid phase strategy. Activation of the pre-loaded 2-chlorotrityl resin was carried out in a fritted polypropylene reaction chamber. 0.1mmol of resin was weighed into the reaction chamber and 2 ml of dry DCM added. The reaction vessel was shaken for 45 minutes. After this time, DCM removed and the resin washed further with DCM. Single couplings were carried out using 5 equivalents of peptide (compared to resin), 5 equivalents of benzotriazol-1-yloxytripyrrolidinophosphonium hexafluorophosphate (PyBOP®), 10 equivalents of N,N-Diisopropylethylamine (DIPEA) and 2 ml of DMF under agitation for 45 minutes. Double peptide couplings were carried out- 2 x 45 minute couplings for each residue addition- the reaction drained after each coupling and fresh reagents added. After each set of coupling reactions, the reaction solution was drained and resin washed with 5 portions of 2 ml DMF. Removal of the Fmoc group was carried out using 5 ml of a solution of 20% piperidine in DMF for 5 under agitation. Piperidine solution was drained and fresh solution added for a further 10 minutes under agitation. Piperidine solution was drained and the resin rinsed using 5 portions of 2 ml DMF. Peptide-resin was treated with a solution of 20% hexafluoroisopropanol in DCM for 1 hour. The resin was removed by filtration and the solvent removed from the filtrate under reduced pressure before precipitation using ether and decanting of the liquid (followed by subsequent ether washes). The resulting solid peptide (Cbz-GPIQ(Trt)-E(tBu)-hPhe-L-OH) was dissolved in deionized water and acetonitrile mix and lyophilized. Purification of peptides was carried out using Perking Elmer HPLC. Samples were injected into a column and a gradient of 0-100% solvent B (solvent A= 95% H_2O, 5% MeCN, 0.01% TFA, solvent B = 95% MeCN, 5%H_2O, 0.01% TFA) over 95 minutes with a flow rate of 2.0 ml/min. Doxorubicin was conjugated to the peptide C-terminus as follows: Doxorubicin.HCl (0.0012 g, 0.002 mol, 1 equiv.), peptide (0.0022 g, 0.002 mol, 1 equiv.), PyBOP® (0.0015 g, 0.003 mol, 1.3 equiv.), and hydroxybenzotriazole hydrate (0.0073 g, 0.0054 mol, 2.6 equiv.) were added together under nitrogen in anhydrous DMF (2 mL). DIPEA (8 equiv., 0.016 mol) was added and the reaction mixture was stirred overnight in the absence of light. Solvent was removed in vacuo and the mixture triturated with cold Et_2O (5 mL) to precipitate the crude peptide which was then obtained through centrifugation to obtain the crude solid peptide conjugate. The product was then purified using a C18 column and reverse phase HPLC (H_2O/MeCN) gradient system using mass spectrometry as confirmation of molecular mass to give a pale red solid (0.0021 g, 70 % yield).

Liquid Chromatography and Mass Spectrometry (LCMS) detection of substrates

LC conditions: High-purity HPLC-grade solvents (Sigma-Aldrich), analytical grade chemicals (Sigma-Aldrich) and triple distilled water were used throughout. Reverse-phase chromatographic separation of substrates was performed using an Acquity UPLC comprising a BEH C18 1.7µM column (2.1mm x 100mm) (Waters, UK).Mobile phases were as follows: Mobile Phase A consisted of 90% HPLC grade water, 10% HPLC grade MeCN and 0.1% HCO2H. Mobile phase B consisted of 40% HPLC grade water, 60% MeCN and 0.1% HCO_2H.

MS conditions: A Micromass ZMD single quadrupole electrospray MS was used in positive mode (Micromass, Manchester, UK) and MassLynx software was used to identify substrates and anticipated metabolites. MS source parameters were optimised to: desolvation gas 375 L/hr, cone gas 33 L/hr, capillary 2.9 kV, sample cone 16V, extraction cone 5V, fR lens 0.1V, source block temperature 150°C and desolvation temperature 200°C. Parent compounds and metabolites were detected as singularly charged ions using selected ion readings (SIR).

Cleavage of substrates by recombinant MMPs

Refer to Method S31

Determination of MMP mRNA expression by semi-quantitative RT-PCR analysis

Refer to Method S32.

MTT assay

Refer to Method S33

Metabolism of **3** in tissues *ex vivo*

Refer to Method S34

ASSOCIATED CONTENT

Supporting Information Availability: Structural analysis of MMP 2 and MMP 9, Fig. S1., Chemical interaction of MMPs with **1** and 3D-docking of MMP-14 with **1**, Fig. S2-S5., Electrospray Ionisation-Liquid Chromatography Mass Spectrometry (ESI-LCMS) identification of **1** and its metabolites, Fig. S6-S9., Synthetic scheme for the production of the peptide doxorubicin conjugates, Fig. S10., 3D and chemical interaction of **2** with MMPs, Fig. S11-S13., LCMS analysis of **2** cleavage by MMPs, Fig. S14-S17., Chemical and 3D interaction of **3** with MMPs, Fig S18-20., LCMS detection of **3** and analysis of its cleavage by MMP-2, MMP-9 and MMP-14, Fig. S21-S24., Metabolism of **3** in tissues *ex vivo*, Fig S25., superimposition of MMP-9 docked with **1**, presented with zinc in the same point of view, Fig S26., Description of *in silico* and *in vitro* methods, Section S27-31., and Embedded Mol2 files. Molecular Formula Strings are also included. This material is available free of charge via the Internet at http://pubs.acs.org.

AUTHOR INFORMATION

Corresponding Author

* David J. Berry, Wolfson Building, School of Medicine, Pharmacy and Health, Durham University, Queen's Campus, Stockton on Tees, TS17 6BH, UK. Email: d.j.berry@durham.ac.uk. Tel: (0044) 1913 340817

Author Contributions\

‡The manuscript was written through contributions of all authors.

ABBREVIATIONS AND ACRONYMS

DCM	Dichloromethane
DIPEA	N,N-Diisopropylethylamine
DMF	Dimethylformamide
Et_2O	Diethyl Ether
HCO_2H	Formic Acid
HPLC	High Performance Liquid Chromatography
HT1080	Human Fibrosarcoma
LCMS	Liquid Chromatography - Mass Spectrometry
MeCN	Acetonitrile
MMPs	Matrix Metalloproteases
MTT	3-(4,5-Dimethylthiazol-2-yl)-2,5-diphenyltetrazolium Bromide
PyBOP	benzotriazol-1-yloxytripyrrolidinophosphonium hexafluorophosphate
TFA	Trifluoroacetic Acid
U87-MG	Human Malignant Glioma

REFERENCES

1. Atkinson, J. M.; Siller, C. S.; and Gill, J. H. Tumour endoproteases: the cutting edge of cancer drug delivery?, *Br. J. Pharmacol.* **2008** *153*, 1344-1352.

2. Vandenbroucke, R. E.; and Libert, C. Is there new hope for therapeutic matrix metalloproteinase inhibition?, *Nat. Rev. Drug. Discov.* **2014** *13*, 904-927.

3. Brown, P. D. Matrix metalloproteinase inhibitors in the treatment of cancer, *Med. Oncol.* **1997** *14*, 1-10.

4. Bourboulia, D.; and Stetler-Stevenson W. G. Matrix metalloproteinases (MMPs) and tissue inhibitors of metalloproteinases (TIMPs): Positive and negative regulators in tumor cell adhesion, *Sem. Cancer Biol.* **2010** *20*, 161-168.

5. Khokha, R.; Murthy, A.; and Weiss, A. Metalloproteinases and their natural inhibitors in inflammation and immunity, *Nat. Rev. Immunol.* **2013** *13*, 649-665.

6. Visse, R.; and Nagase, H. Matrix metalloproteinases and tissue inhibitors of metalloproteinases: structure, function, and biochemistry, *Circ. Res.* **2003** *92*, 827-839.

7. Clark, I. A.; Swingler, T. E.; Sampieri, C. L.; and Edwards, D. R. The regulation of matrix metalloproteinases and their inhibitors, *Int. J. Biochem. Cell Biol.* **2008** *40*, 1362-1378.

8. Nagase, H.; Visse, R.; and Murphy, G. Structure and function of matrix metalloproteinases and TIMPs, *Cardiovasc. Res.* **2006** *69*, 562-573.

9. Shay, G.; Lynch, C. C.; and Fingleton, B. Moving targets: Emerging roles for MMPs in cancer progression and metastasis, *Matrix Biol. : J. Int. Soc. Matrix Biol.* **2015** *44-46*, 200-206.

10. Hu, J.; Van den Steen, P. E.; Sang, Q. X.; and Opdenakker, G. Matrix metalloproteinase inhibitors as therapy for inflammatory and vascular diseases, *Nat. Rev. Drug Discov.* **2007** *6*, 480-498.

11. Pirard, B. Insight into the structural determinants for selective inhibition of matrix metalloproteinases, *Drug Discov. Today* **2007** *12*, 640-646.

12. Overall, C. M.; and Kleifeld, O. Tumour microenvironment - opinion: validating matrix metalloproteinases as drug targets and anti-targets for cancer therapy, *Nat. Rev. Cancer* **2006** *6*, 227-239.

13. Mccullagh, K.; Wadsworth, H.; and Hann, M. Carboxyalkyl peptide derivatives, Google Patents, EP 0126974 A1 **1985.**

14. De, B.; Natchus, M. G.; Cheng, M., Pikul, S.; Almstead, N. G.; Taiwo, Y. O.; Snider, C. E., Chen, L.; Barnett, B., Gu, F.; and Dowty, M. The next generation of MMP inhibitors. Design and synthesis, *Ann. N. Y. Acad. Sci.* **1999** *878*, 40-60.

15. Overall, C. M.; and Kleifeld, O. Towards third generation matrix metalloproteinase inhibitors for cancer therapy, *Br. J. Cancer* **2006** *94*, 941-946.

16. Coussens, L. M.; Fingleton, B.; and Matrisian, L. M. Cancer therapy - Matrix metalloproteinase inhibitors and cancer: Trials and tribulations, *Science* **2002** *295*, 2387-2392.

17. Dufour, A.; and Overall, C. M. Missing the target: matrix metalloproteinase antitargets in inflammation and cancer, *Trends Pharmacol. Sci.* **2013** *34*, 233-242.

18. Georgiadis, D.; and Dive, V. Phosphinic peptides as potent inhibitors of zinc-metalloproteases, *Top. Curr. Chem.* **2015** *360*, 1-38.

19. Jacobsen, J. A.; Major Jourden, J. L.; Miller, M. T.; and Cohen, S. M. To bind zinc or not to bind zinc: an examination of innovative approaches to improved metalloproteinase inhibition, *Biochim. Biophys. Acta* **2010** *1803*, 72-94.

20. Heal, W. P.; Wickramasinghe, S. R.; and Tate, E. W. Activity based chemical proteomics: profiling proteases as drug targets, *Curr. Drug Discov. Technol.* **2008** *5*, 200-212.

21. Chuang, C. H.; Chuang, K. H.; Wang, H. E.; Roffler, S. R.; Shiea, J. T.; Tzou, S. C.; Cheng, T. C.; Kao, C. H.; Wu, S. Y.; Tseng, W. L.; Cheng, C. M.; Hou, M. F.; Wang, J. M.; and Cheng, T. L. In vivo positron emission tomography imaging of protease activity by generation of a hydrophobic product from a noninhibitory protease substrate, *Clin. Cancer Res.* **2012** *18*, 238-247.

22. Atkinson, J. M.; Falconer, R. A.; Edwards, D. R.; Pennington, C. J.; Siller, C. S.; Shnyder, S. D.; Bibby, M. C.; Patterson, L. H.; Loadman, P. M.; and Gill, J. H. Development of a novel tumor-targeted vascular disrupting agent activated by membrane-type matrix metalloproteinases, *Cancer Res.* **2010** *70*, 6902-6912.

23. Vandooren, J.; Opdenakker, G.; Loadman, P. M.; and Edwards, D. R. Proteases in cancer drug delivery, *Adv. Drug Deliv. Rev.* **2016** *97*, 144-155.

24. Choi, K. Y.; Swierczewska, M.; Lee, S.; and Chen, X. Protease-activated drug development, *Theranostics* **2012** *2*, 156-178.

25. Ansari, C.; Tikhomirov, G. A.; Hong, S. H.; Falconer, R. A.; Loadman, P. M.; Gill, J. H.; Castaneda, R.; Hazard, F. K.; Tong, L.; Lenkov, O. D.; Felsher, D. W.; Rao, J.; and Daldrup-Link, H. E. Development of novel tumor-targeted theranostic nanoparticles activated by membrane-type matrix metalloproteinases for combined cancer magnetic resonance imaging and therapy, *Small* **2014** *10*, 566-575, 417.

26. Wang, Y.; Pu, L.; Li, Z.; Hu, X.; and Jiang, L. Hypoxia-inducible factor-1alpha gene expression and apoptosis in ischemia-reperfusion injury: a rat model of early-stage pressure ulcer, *Nurs. Res.* **2016** *65*, 35-46.

27. Huggins, D. J.; Sherman, W.; and Tidor, B. Rational approaches to improving selectivity in drug design, *J. Med. Chem.* **2012** *55*, 1424-1444.

28. Rowsell, S.; Hawtin, P.; Minshull, C. A.; Jepson, H.; Brockbank, S. M.; Barratt, D. G.; Slater, A. M.; McPheat, W. L.; Waterson, D.; Henney, A. M.; and Pauptit, R. A. Crystal structure of human MMP9 in complex with a reverse hydroxamate inhibitor, *J. Mol. Biol.* **2002** *319*, 173-181.

29. Dhanaraj, V.; Ye, Q-Z.; Johnson, LL.; Hupe, DJ.; Ortwine, DF.; Dunbar, JB.; Rubin, JR.; Pavlovsky, A.; Humblet, C.; and Blundell, TL. X-ray structure of gelatinase A catalytic domain complexed with a hydroxamate inhibitor, *Croat. Chem. Acta* **1999** *72*, 575-591.

30. Fernandez-Catalan, C.; Bode, W.; Huber, R.; Turk, D.; Calvete, JJ.; Lichte, A.; Tschesche, H., and Maskos, K. Crystal structure of the complex formed by the membrane type 1-matrix metalloproteinase with the tissue inhibitor of metalloproteinase-2, the soluble progelatinase A receptor, *Embo J.* **1998** *17*, 5238-5248.

31. Maskos, K. Crystal structures of MMPs in complex with physiological and pharmacological inhibitors, *Biochimie* **2005** *87*, 249-263.

32. Bickett, D. M.; Green, M. D.; Berman, J.; Dezube, M.; Howe, A. S.; Brown, P. J.; Roth, J. T.; and McGeehan, G. M. A high throughput fluorogenic substrate for interstitial collagenase (MMP-1) and gelatinase (MMP-9), *Anal. Biochem* **1993**. *212*, 58-64.

33. Albright, C. F.; Graciani, N.; Han, W.; Yue, E.; Stein, R., Lai, Z.; Diamond, M.; Dowling, R.; Grimminger, L.; Zhang, S. Y.; Behrens, D.; Musselman, A.; Bruckner, R.; Zhang, M.; Jiang, X.; Hu, D.; Higley, A.; Dimeo, S.; Rafalski, M.; Mandlekar, S.; Car, B.; Yeleswaram, S.; Stern, A.; Copeland, R. A.; Combs, A.; Seitz, S. P.; Trainor, G. L.; Taub, R.; Huang, P.; and Oliff, A. Matrix metalloproteinase-activated doxorubicin prodrugs inhibit HT1080 xenograft growth better than doxorubicin with less toxicity, *Mol. Cancer Ther.* **2005** *4*, 751-760.

34. Hu, Z.; Jiang, X.; Albright, C. F.; Graciani, N.; Yue, E.; Zhang, M.; Zhang, S. Y.; Bruckner, R.; Diamond, M.; Dowling, R.; Rafalski, M.; Yeleswaram, S.; Trainor, G. L.; Seitz, S. P.; and Han, W. Discovery of matrix metalloproteases selective and activated peptide-doxorubicin prodrugs as anti-tumor agents, *Bioorg. Med. Chem. Lett.* **2010** *20*, 853-856.

35. Atkinson, J. M.; Falconer, R. A.; Edwards, D. R.; Pennington, C. J.; Siller, C. S.; Shnyder, S. D.; Bibby, M. C.; Patterson, L. H.; Loadman, P. M.; and Gill, J. H. Development of a novel tumor-targeted vascular disrupting agent activated by MT-MMPs, *Cancer Res.* **2010** *17*, 6902-6912.

36. Kridel, SJ.; Sawai, H.; Ratnikov, BI.; Chen, EI.; Li, W.; Godzik, A.; Strongin, AY.; and Smith, JW. A unique substrate binding mode discriminates membrane type-I matrix metalloproteinase from other matrix metalloproteinases. *J. Biol. Chem.* **2002** *277*, 23788-23793.

37. McClellan, M.; Benner, J.; Schilsky, R.; Epstein, D.; Woosley, R.; Friend, S.; Sidransky, D.; Geoghegan, C.; and Kessler, D. An accelerated pathway for targeted cancer therapies, *Nat. Rev. Drug Discov.* **2011** *10*, 79-80.

38. Santiskulvong, C.; and Rozengurt, E. Galardin (GM6001), a broad-spectrum matrix metalloproteinase inhibitor, blocks bombesin- and LPA-induced EGF receptor tranactivation and DNA synthesis in rat-1 cells. *Exp. Cell Res.* **2003** *290*, 437-446.

39. Wang, H.; Xu, T.; Jiang, Y.; Xu, H.; Yan, Y.; Fu, D.; and Chen, J. The challenges and the promise of molecular targeted therapy in malignant gliomas, *Neoplasia* **2015** *17*, 239-255.

40. Vartak, D. G.; and Gemeinhart, R. A. Matrix metalloproteases: underutilized targets for drug delivery, *J. Drug Target* **2007** *15*, 1-20.

41. Cathcart, J.; Pulkoski-Gross, A.; and Cao, J. Targeting matrix metalloproteinases in cancer: bringing new life to old ideas, *Genes Dis.* **2015** *2*, 26-34.
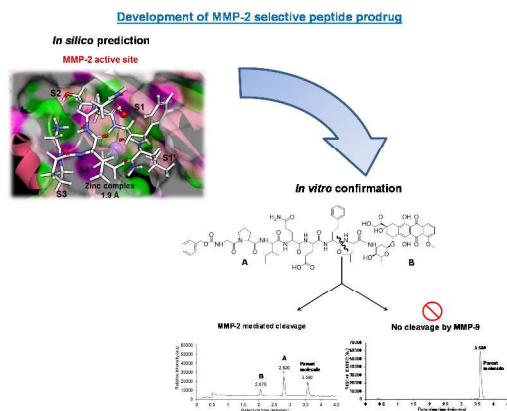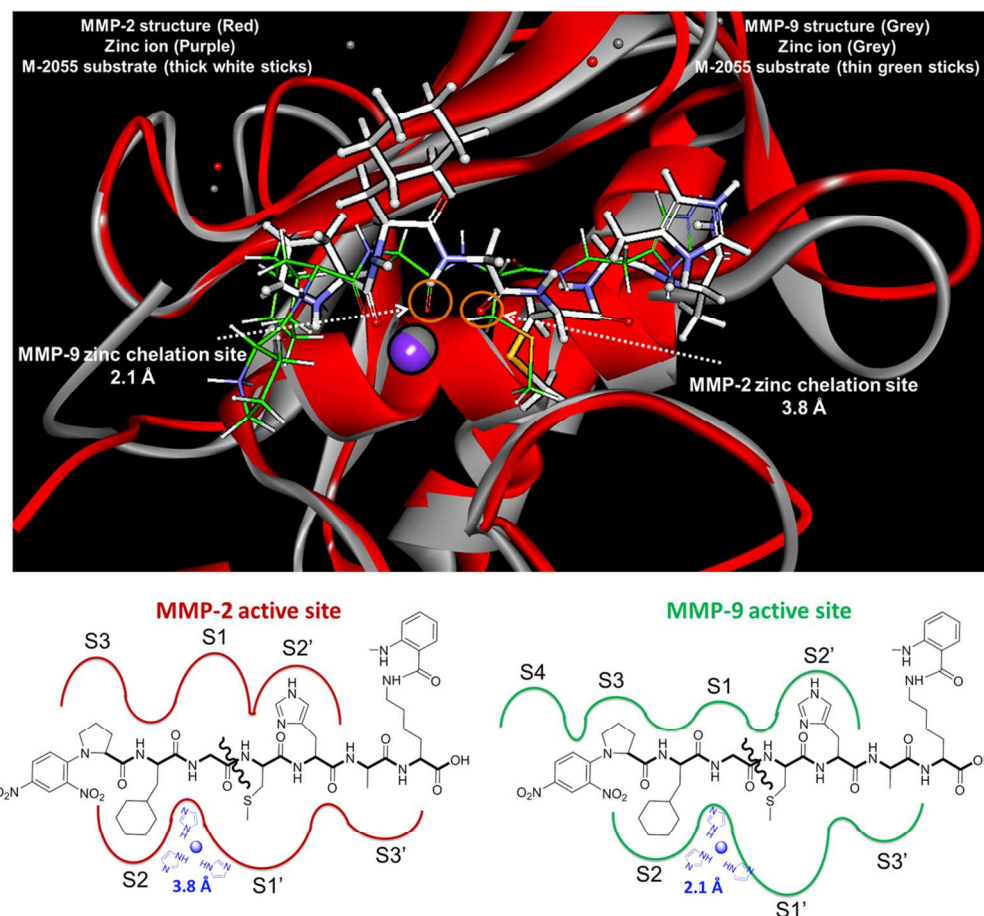
For Table of Contents Only

Figure 1. (Top) Stereo view of the docked complexes of 1 sub-strate and the catalytic domain of human MMP-2 (PDB ID: 1QIB) and MMP-9 (PDB ID: 1GKC). The MMP-substrate docked complexes are merged with zinc as the same point of view. MMP-2 structure is shown in red, zinc as purple and 1 substrate (white sticks) docked within MMP-2 active site. MMP-9 is shown in grey, zinc as green and 1 substrate (thin green sticks) docked within its active site. (Bottom) Schematic representation of 1: active site binding interaction in human MMP-2 and MMP-9. MMP-2 and MMP-9 enzyme binding pockets are shown in red and green respectively. Substrate chemical structure and its scissile bond is shown in black. The zinc ion is indicated in blue.
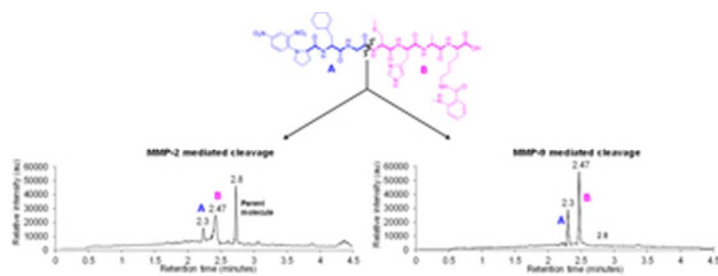
52x48mm (600 x 600 DPI)

Figure 2. Schematic representation of the cleavage of 1 substrate by recombinant MMP-2 and MMP-9 enzymes at Gly-Cys(Me).
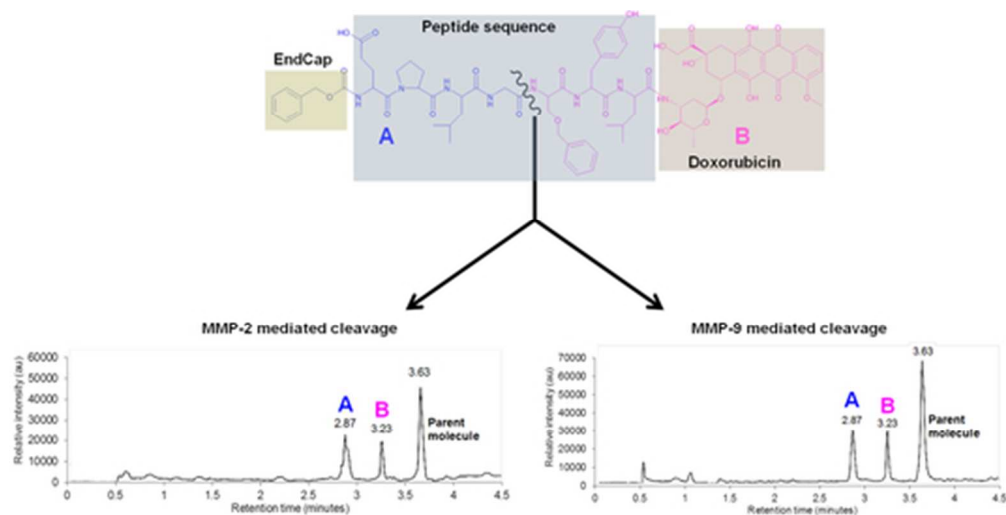
15x5mm (600 x 600 DPI)

Figure 3. Schematic representation of the cleavage of 2 by re-combinant MMP-2 and MMP-9 enzymes at the Gly-Ser(O-Bn) bond.

22x11mm (600 x 600 DPI)

1
2
3
4
5
6
7
8
9
10
11
12
13
14
15
16
17
18
19
20
21
22
23
24
25
26
27
28
29
30
31
32
33
34
35
36
37
38
39
40
41
42
43
44
45
46
47
48
49
50
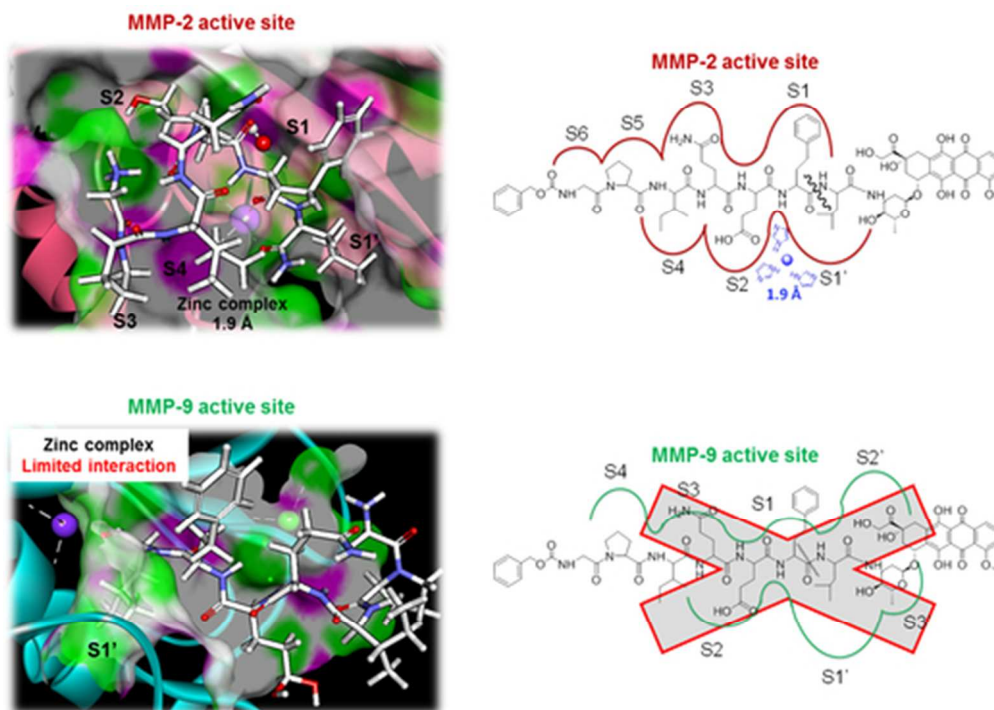51
52
53
54
55
56
57
58
59
60

Figure 4. (Left) Stereo view of docked complexes of 3 (white sticks), catalytic domain of human MMP-2 (PDB ID: 1QIB) (Red) and MMP-9 (PDB ID: 1GKC) (Green). Catalytic and structural zinc ions are shown as purple spheres and active-site cleft residues (αβ-helix loop and the specificity loop) are shown as green. (Right) Schematic representation of 3 substrate: active site binding interaction in MMP-2 and MMP-9, are shown in red and green respectively. Substrate chemical structure and its scissile bond is shown in black and zinc ion coordinated by histidine is indicated in blue.
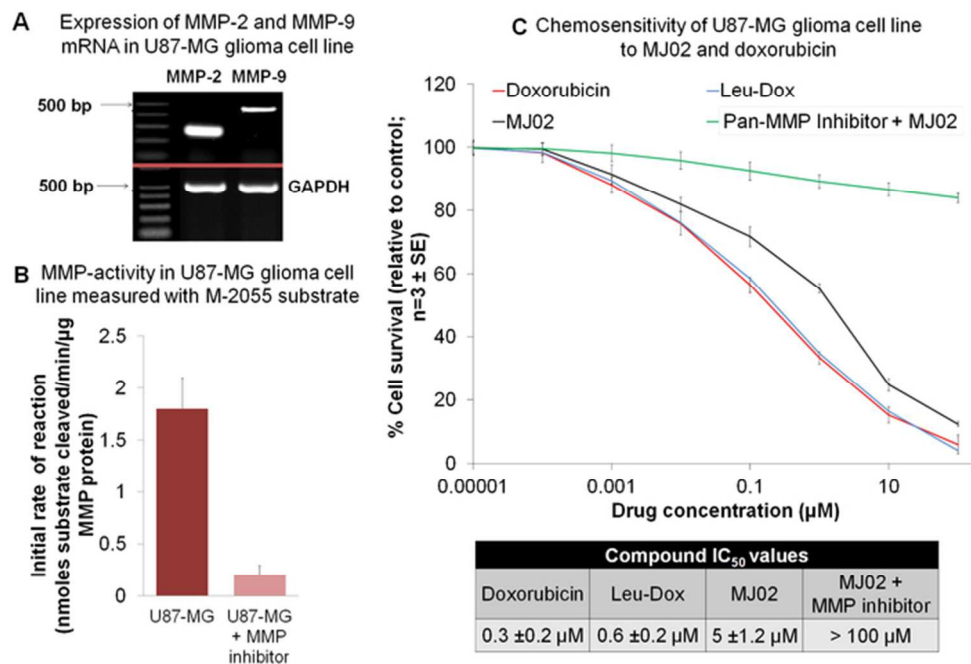
22x15mm (600 x 600 DPI)

A Expression of MMP-2 and MMP-9 mRNA in U87-MG glioma cell line

MMP-2 MMP-9

500 bp →

500 bp → GAPDH

B MMP-activity in U87-MG glioma cell line measured with M-2055 substrate

Initial rate of reaction (nmoles substrate cleaved/min/µg MMP protein)

U87-MG   U87-MG + MMP inhibitor

C Chemosensitivity of U87-MG glioma cell line to MJ02 and doxorubicin

— Doxorubicin   — Leu-Dox
— MJ02   — Pan-MMP Inhibitor + MJ02

% Cell survival (relative to control; n=3 ± SE)

Drug concentration (µM)

Compound IC$_{50}$ values			
Doxorubicin	Leu-Dox	MJ02	MJ02 + MMP inhibitor
0.3 ±0.2 µM	0.6 ±0.2 µM	5 ±1.2 µM	> 100 µM

Figure 5. Therapeutic activity of 3 against human cancer. A) Expression of MMP-2 and MMP-9 mRNA in the U87-MG glio-ma cell line; B) MMP-activity in the U87-MG cell line, as demonstrated by activation of 1 substrate Dnp-Pro-β-cyclohexyl-Ala-Gly-Cys(Me)-His-Ala-Lys(N-Me-Abz)-NH2; C) Cytotoxicity of doxorubicin, Leu-Dox and 3 against U87-MG cell line. MMP-selective activation of 3 in the presence of a pan-MMP inhibitor (Ilomastat).

30x20mm (600 x 600 DPI)